Eur Biophys J (2011) 40:1087–1100
DOI 10.1007/s00249-011-0726-z

ORIGINAL PAPER

Investigating the effect of a single glycine to alanine substitution on interactions of antimicrobial peptide latarcin 2a with a lipid membrane

Grace Idiong · Amy Won · Annamaria Ruscito · Bonnie O. Leung · Adam P. Hitchcock · Anatoli Ianoul

Received: 18 March 2011 / Revised: 3 June 2011 / Accepted: 12 June 2011 / Published online: 7 July 2011
© European Biophysical Societies' Association 2011

Abstract Latarcins are linear, α-helical antimicrobial peptides purified from the venom of the Central Asian spider *Lachesana tarabaevi*, with lytic activity against Gram-positive and Gram-negative bacteria, erythrocytes, and yeast at micromolar concentrations. In this work, we investigated the role of the hinge in latarcin 2a (ltc2a, GLFGKLIKKFGRKAISYAVKKARGKH-COOH), which adopts a helix–hinge–helix conformation in membrane-mimicking environments, on peptide–membrane interactions and its potential effect on the selective toxicity of the peptide. A modified latarcin 2a, ltc2aG11A, obtained by replacing the glycine at position 11 with alanine (ltc2aG11A, GLFGKL IKKFARKAISYAVKKARGKH-COOH), adopts a more rigid structure due to the reduced conformational flexibility. Langmuir monolayer measurements combined with atomic force microscopy and X-ray photoemission electron microscopy (X-PEEM) indicate that both peptides bind and insert preferentially into anionic compared with zwitterionic phospholipid monolayers. Modified ltc2aG11A was found to be more disruptive of supported phospholipid bilayer modeling mammalian cell membrane. However, no considerable difference in lytic activity of the two peptides toward bacterial membrane was found. Overall the data indicate that decrease in the flexibility of ltc2a induced by the modification in the hinge region is likely to increase the peptide's nonspecific interactions with zwitterionic cell membranes and potentially increase its toxicity against eukaryotic cells.

Keywords Antimicrobial peptides · Phospholipid · Monolayer · Atomic force microscopy · Model cell membrane · X-ray photoemission electron microscopy

G. Idiong · A. Won · A. Ruscito · A. Ianoul (✉)
Department of Chemistry, Carleton University,
1125 Colonel By Dr., Ottawa, ON K1S 5B6, Canada
e-mail: anatoli_ianoul@carleton.ca

B. O. Leung · A. P. Hitchcock
Brockhouse Institute for Materials Research,
McMaster University, Hamilton, ON L8S 4M1, Canada

Introduction

Antimicrobial peptides (AMP) represent a wide range of short, cationic, amphipathic peptides that are an important component of the natural defense of most living organisms against invading pathogens. They have been isolated and characterized from tissues and cell types ranging from prokaryotes to humans (Yeaman and Yount 2003; Reddy et al. 2004; Hancock and Sahl 2006; Zasloff 2002). Prolonged use of antibiotics has led to a steady increase in antibiotic-resistant bacterial strains. Due to this increased resistance, AMP attract considerable interest for their potential applications (Yeaman and Yount 2003; Shlyapnikov et al. 2008; Zhang and Falla 2010; Guani-Guerra et al. 2010). These peptides exhibit broad-spectrum activity against Gram-positive and Gram-negative pathogens (Yeaman and Yount 2003; Reddy et al. 2004). One of the major hindrances to wide application of AMP-based drugs is the selective toxicity of different antimicrobial peptides (Yeaman and Yount 2003; Shlyapnikov et al. 2008). The ability to kill microorganisms without harming the host is an essential requirement for any antimicrobial agent.

Among the five main parameters (conformation, amphipathicity, charge, hydrophobicity, and polar angle) that define the antimicrobial activity and selective toxicity of such peptides, conformation is often used to classify AMP.

Linear α-helical peptides represent one of the main structural groups (Yeaman and Yount 2003; Zasloff 2002). α-Helical antimicrobial peptides are usually unstructured in solution and only become helical when interacting with phospholipid membranes. Upon this conformational change the peptides become highly amphipathic, with distinct hydrophilic and hydrophobic surfaces (Yeaman and Yount 2003). The amphipathicity of an AMP influences peptide activity against negatively charged membranes and, to a high degree, increases peptide lytic activity towards zwitterionic or neutral membranes (Yeaman and Yount 2003). The charge of antimicrobial peptides is critical with regards to the initial electrostatic attraction of antimicrobial peptides to negatively charged phospholipid membranes of pathogens (Yeaman and Yount 2003). On the other hand, hydrophobicity dictates the extent to which a peptide can insert into the lipid bilayer, and high levels of hydrophobicity can cause mammalian cell toxicity and loss of antimicrobial specificity (Yeaman and Yount 2003).

The mechanisms by which antimicrobial peptides disrupt the membrane bilayer during binding significantly influence their antimicrobial activity and/or selective toxicity (Yeaman and Yount 2003). The three mechanisms that are the foundation for all proposed models are the barrel-stave, the toroidal-pore, and the carpet mechanism. The barrel-stave mechanism represents peptides that insert into the membrane and self-aggregate into pores (Yeaman and Yount 2003; Brogden 2005; Melo et al. 2009). In the toroidal-pore mechanism, the phospholipid membrane bends, allowing self-association and more peptide interaction so that the pore is formed partially by the inserted peptides and partially by phospholipid head groups. Lastly, the carpet mechanism describes peptides that do not form pores but actually accumulate on the surface parallel to the membrane, destabilizing the phospholipid packing and disrupting the membrane, which eventually leads to formation of micelles (Yeaman and Yount 2003; Brogden 2005; Melo et al. 2009).

A large number of promising therapeutic agents have been isolated from natural venoms (Kozlov et al. 2006; Liu et al. 2009). Recently, a new family of antimicrobial peptides referred to as latarcins was purified from the venom gland of the Central Asian spider *Lachesana tarabaevi* (Kozlov et al. 2006). These antimicrobial peptides form seven structurally unrelated groups of short linear cysteine-free, membrane-active molecules that are found to produce lytic effects on Gram-positive (e.g., *Bacillus subtilis*) and Gram-negative (e.g., *Escherichia coli*) bacteria, erythrocytes, and yeast at micromolar concentrations and share little homology with other known peptides. The two latarcins that have been studied extensively so far are latarcin 1 (ltc1) and latarcin 2a (ltc2a).

Ltc1 is a 26-amino-acid-residue peptide that has net charge of +10, strong antibacterial activity [minimum inhibitory concentration (MIC) value in the 0.5–5 μM range against Gram-positive and Gram-negative bacteria] and moderate hemolytic activity (MIC value of 80 μM against rabbit erythrocytes, Kozlov et al. 2006). The ltc1 peptide was found to form a single amphipathic helix in membrane-mimicking environments, with narrow-shaped hydrophobicity surface and no hydrophobicity gradient along the axis (Dubovskii et al. 2008). As a result, in the cell membrane the peptide is believed to adopt a transmembrane orientation under conditions of applied potential and form variable-sized lesions.

Ltc2a is a 26-amino-acid-residue (GLFGKLIKKFGR KAISYAVKKARGKH-COOH) peptide that exhibits a broad spectrum of antibacterial activity against *B. subtilis* and *E. coli* with MIC values in the 0.5–7 μM range (Kozlov et al. 2006). At the same time the peptide has comparatively strong hemolytic activity (6 μM caused 20% lysis of rabbit erythrocytes). Ltc2a was found to adopt a helix–hinge–helix conformation in membrane-mimicking environments with a hydrophobicity gradient along the peptide sequence (Dubovskii et al. 2006). The N-terminal helix was shown to be buried in the membrane, with the C-terminal helix lying nearly parallel to the membrane surface. Unlike ltc1, ltc2a was found to act by the carpet-like mechanism (Kozlov et al. 2006). The difference in the hemolytic activity between the two peptides is suggested to result from the different secondary structure and organization of hydrophobic domains within the folded peptides (Dubovskii et al. 2006, 2008; Polyansky et al. 2009). An effort was made to modify the structure of ltc2a in such a way as to alter the hydrophobicity pattern and minimize its cytotoxicity (Polyansky et al. 2009). Of particular interest are modifications within the hinge region of ltc2a.

The helix–hinge–helix structure found in ltc2a often occurs in cationic antimicrobial peptides longer than 20 amino acid residues. More often, one of the helices is found to enter the membrane while the other helix is positioned parallel to the membrane surface with the help of some hydrophobic residues, such as Phe or Trp, that anchor to the membrane (Melo et al. 2009; Oh et al. 2000; Ibrahim et al. 2001; Van Khan et al. 2001; Pukala et al. 2004, 2007; Lee et al. 2007). Small modifications in the hinge region were found to have a dramatic effect on the peptide's activity (Polyansky et al. 2009; Van Khan et al. 2001; Pukala et al. 2004, 2007; Lee et al. 2007). This effect is primarily due to the loss of conformational flexibility, which in turn prevents the peptides from binding and penetrating deeper into the bilayer; for example, the helix–hinge–helix structural feature was found to play a critical role in the activity of a hybrid peptide incorporating cecropin and magainin 2 residues, since deletion of the

hinge sequence resulted in a significant decrease in bactericidal and tumoricidal activities (Oh et al. 2000). The helix–hinge–helix structure was found to be an important prerequisite for the antimicrobial activity of a peptide derived from lysozyme with the N-terminal helix partitioning into the hydrophobic portion of lipid bilayer (Ibrahim et al. 2001). Replacement of glycines with alanines was used to study the effect of conformational flexibility on the activity of clavanin A, which demonstrated the functional importance of the two hinge regions present in the peptide (Van Khan et al. 2001). The hinge region was also found to play an important role in effectively orientating the two helices of antimicrobial peptides caerin 1.1 (Pukala et al. 2004) and cupiennin 1a (Pukala et al. 2007). For piscidin 1, conformational flexibility induced by the introduction of a hinge region was found to be a critical factor for bacterial cell selectivity (Lee et al. 2007).

In the present study, wild-type ltc2a and ltc2aG11A, a derivative obtained by replacing the glycine at position 11 (the hinge region) with alanine, were compared in their ability to bind and rupture model cell membranes. In contrast to glycine, alanine favors the helix conformation (Chakrabartty et al. 1991; Rohl et al. 1999; Okamoto and Hansmann 1995; Javadpour et al. 1999; Li and Deber 1994) and cannot adopt the same set of (ϕ, ψ) angles. Therefore, it is expected that the modified ltc2aG11A (GLFGKLIKKF**A**RKAISYAVKKARGKH-COOH) will adopt a more rigid structure. We used Langmuir monolayer techniques combined with atomic force microscopy (AFM) and X-ray photoemission electron microscopy (X-PEEM) to investigate the role of the hinge region in latarcin interactions with phospholipid monolayers and bilayers as model cell membranes. Carboxyfluorescein leakage assay was used to determine the difference in membrane rupturing activity between the peptides. Results of this work demonstrate the effect of point mutations on the physicochemical and membrane-binding properties of antimicrobial peptides.

Materials and methods

Chemicals

1,2-Dipalmitoyl-*sn*-glycero-3-phosphocholine (DPPC), 1,2-dipalmitoyl-*sn*-glycero-3-[phospho-*rac*-(1-glycerol)] (DPPG), 1,2-dioleoyl-*sn*-glycero-3-phosphoethanolamine (DOPE), 1,2-dioleoyl-*sn*-glycero-3-phospho-(1′-*rac*-glycerol) (sodium salt) (DOPG), 1,2-dioleoyl-*sn*-glycero-3-phosphocholine (DOPC), 1,1′,2,2′-tetramyristoyl cardiolipin (sodium salt) (CL), egg sphingomyelin (SPM), cholesterol (Chol, ovine wool, >98%), and *E. coli* total lipid extract were purchased from Avanti Polar Lipids Inc. Solutions (1 mg/ml) of the lipids were prepared in chloroform (spectroscopy grade, Caledon)/methanol (reagent grade, Caledon) (3:1, v/v) mixture. Latarcin 2a (M.W. 2902.60, >95.4% purity) and latarcin 2a G11A (M.W. 2916.57, >95.1% purity) were synthesized by Gen Script Corporation. Stock solutions of the peptides were prepared at the required concentration (usually 5 mg/ml) in chloroform/methanol (1:1, v/v) mixture or in 18.2 MΩ cm Milli-Q water. 2,2,2-Trifluoroethanol (TFE, >99.0%) was purchased from Sigma–Aldrich.

Methods

Langmuir monolayer experiments

Monolayers were prepared on a Langmuir–Blodgett (LB) trough (NIMA 311-D, Coventry, UK) using ~200 ml phosphate-buffered saline (PBS, 0.01 M, 138 mM NaCl, 2.7 mM KCl, Sigma–Aldrich), pH 7.4 as the subphase at room temperature (23°C). The monolayers were prepared by spreading 30 µl of the 1 mg/ml solution of lipid, peptide or 1/1 mixture at the air–water interface drop by drop. After a solvent evaporation period of 20 min, the monolayer was formed by two compression–expansion isotherm cycles. Pressure–area isotherms were recorded with a barrier speed of 10 cm^2/min. The monolayer was compressed to the desired pressure and transferred onto freshly cleaved mica (1 × 1″ Hi-Grade Mica; Ted Pella, Inc., Redding, CA) at 1 mm/min with transfer ratios of 60–100%.

To determine the critical pressure of insertion (CPI), a round polytetrafluoroethylene (PTFE) dish (surface area 5.67 cm^2) with 20 ml PBS as subphase was used. The CPI for different lipid monolayers was determined by preparing a monolayer of a desired lipid mixture at a desired initial pressure, π, and adding the peptide into the trough through a small opening in a dish to obtain the final peptide concentration close to MIC (Kozlov et al. 2006). Increase in the pressure, $\Delta\pi$, upon peptide addition was then plotted as a function of initial surface pressure, π. The data points were further fitted using a linear function. Extrapolation at zero change in pressure ($\Delta\pi = 0$) gives the CPI. Effect of volume increase on the surface pressure was insignificant, as determined by injecting the same volume of buffer without the peptide.

Carboxyfluorescein leakage assay

For this assay five different model cell membranes were used: DPPC, DPPG, *E. coli* model (DOPE/DOPG 80/20 mol%), *Staphylococcus aureus* model (DOPG/CL 55/45 mol%), and *B. subtilis* model (DOPE/DOPG/CL 12/84/4 mol%) (Epand et al. 2007). Large unilamellar vesicles were prepared by dissolving the appropriate

amount of lipid in chloroform, drying the solvent under a stream of nitrogen, and keeping the sample under vacuum for at least 24 h to ensure complete solvent removal. The obtained lipid films were hydrated in leakage buffer [10 mM Tris–HCl (Bioshop), 150 mM NaCl, 1 mM ethylenediamine tetraacetic acid (EDTA, Bioshop) pH 7.45 in 18.2 MΩ cm MilliQ water] containing 70 mM carboxyfluorescein [(6)-carboxyfluorescein (ACROS Organic)] for 30 min (at 55°C for DPPC and DPPG, and at 30°C for bacterial model membranes) to obtain final lipid concentration of 1 mg/ml. Lipid suspensions were then sonicated with Elma S10H Elmasonic for 20 min. Five freeze–thaw cycles were performed to maximize carboxyfluorescein encapsulation. The lipid suspension was further extruded through 100-nm polycarbonate membrane (Nuclepore Track-Etch membrane, Whatman) 30 times (at 55°C for DPPC and DPPG, and at 30°C for bacterial model membranes). Free carboxyfluorescein was separated from encapsulated with a Sephadex G-50 size exclusion column using leakage buffer for equilibrium and elution.

Leakage experiments were carried out using 2 ml carboxyfluorescein-containing vesicles diluted 10 times with the leakage buffer on a Varian Cary Eclipse spectrofluorimeter. Measurements were carried out with excitation and emission wavelengths determined for each experiment (490–500 nm and 518–521 nm, excitation and emission, respectively). Excitation and emission slits were 2.5 nm, photomultiplier tube voltage was 540 V, and integration time was 1.0 s. Baseline fluorescence (F_0) was monitored before addition of the peptide for 30 s. After the peptide was added, the fluorescence signal intensity was monitored for approximately 15 min or until no further changes occurred. The final fluorescence signal intensity (F) was then measured. To determine the maximum fluorescence signal corresponding to complete disruption of the vesicles (F_M), 20 µl 10% Triton X-100 (Bioshop) was added to the mixture at the end of the experiment and fluorescence intensity increase was monitored for 5 min. The leakage fraction was calculated as: % leakage $= [(F - F_0) \times 100\%]/(F_M - F_0)$.

The concentration of lipid phosphorus was measured by phosphate assay (Won and Ianoul 2009). Vesicles with carboxyfluorescein (300 µl) were mixed with 1 ml $HClO_4$ and heated with a block heater for 1 h. After cooling, 4.6 ml 0.22% ammonium molybdate (Bioshop) and 0.2 ml Fiske–Subbarow reducing agent were added, followed by vigorous stirring. The solution was incubating in a water bath at 100°C for 15 min. Absorption of the signal at 817 nm was measured. Fiske–Subbarow reagent was prepared by mixing 40 ml 15% (w/v) sodium bisulfate (Acros Organic), 0.2 g sodium sulfite (Bioshop), and 0.1 g 1-amino-4-naphtholsulfonic acid (Ricca Chemical Company). The solution was filtered and stored in the dark at 4°C. Standard phosphate solutions were prepared using sodium phosphate monobasic up to 1 mM in 18.2 MΩ cm MilliQ water.

AFM imaging

Topography images of monolayers were obtained using an Ntegra (NTMDT, Russia) atomic force microscope in semicontact mode in air at 23°C with 512 × 512 points per image. A 100 × 100 μm^2 scanner (Ntegra) and cantilevers with rotated monolithic silicon tips (125 µm long, 40 N/m spring constant Tap 300Al, resonance frequency 315 kHz; Budget Sensors) were used for all topographic measurements. The typical scan rate was 0.5 Hz. At least three areas of the same sample were imaged for several independent sample preparations.

For experiments with phospholipid bilayers, appropriate amounts of DOPC, SPM, and Chol were weighed and dissolved in chloroform. Lipid mixture was then dried under a stream of nitrogen and kept under vacuum for more than 24 h to ensure total solvent evaporation. The obtained lipid film was hydrated with PBS at 50°C for 30 min to prepare 1 mg/ml vesicle suspension. The suspension was further sonicated at 50°C until the mixture became clear. Supported lipid bilayers (SLB) were formed on freshly cleaved mica sheet substrates sealed with a silicon O-ring in a fluid cell (NTMDT) by adding 1 ml PBS, 40 µl 1 M $CaCl_2$, and 1 ml lipid vesicles (1 mg/ml). After 50 min of incubation at room temperature, the fluid cell was rinsed with 20 ml PBS and with MilliQ deionized water to remove excess vesicles. After the topography of SLB was verified with AFM, 15–30 µl ltc2a or ltc2aG11A was added to the liquid cell to obtain final peptide concentration around 2.9 µg/ml (1 µM) and incubated with the bilayer for 30 min at room temperature. The sample was then extensively rinsed with deionized water to ensure complete removable of excess peptide.

AFM topography images of SLB in MilliQ deionized water were obtained at room temperature in contact mode. Cantilevers with rotated monolithic silicon tips (450 µm-long, force constant 0.2 N/m ContAl, resonant frequency 13 kHz; Budget Sensors) were used for all topographic measurements with scan rate between 0.35 and 0.65 Hz. At least three different areas (pre and post peptide addition) were imaged for each sample preparation.

X-PEEM imaging

All X-PEEM measurements were performed at the Advanced Light Source (ALS) on bend magnet beamline 7.3.1 (PEEM-2). Detailed accounts of the experimental apparatus, beamline setup, instrument optics, and data analysis have been presented previously (Leung et al.

2009). C 1s image stacks were aligned, normalized to the ring current, and divided by the I_0 spectrum collected from a clean, HF-etched Si(111) chip. All stacks were calibrated externally by assigning the C 1s → π^* transition of polystyrene to 285.15 eV. Each pixel of the C 1s image stacks were fitted to DPPC, DPPG or latarcin 2a reference spectra using singular value decomposition (SVD), which is an optimized method for least-squares refinement in over-determined data sets (Koprinarov et al. 2002). DPPC and DPPG near-edge X-ray absorption fine structure (NEXAFS) reference spectra were obtained experimentally using the polymer scanning transmission X-ray microscope (STXM) at ALS beamline 5.3.2. The latarcin 2a reference spectrum was predicted using the X-Spec Sim widget in the aXis2000 (http://www.unicorn.mcmaster.ca/aXis2000) software program, which has previously been shown to exhibit good correlation between simulated and experimental spectra of peptides and proteins (Stewart-Ornstein et al. 2007). The fit coefficients generated from the SVD analysis are presented as component maps, which are the spatial distributions of each component. Quantitative results were obtained by extracting the average NEXAFS spectrum from lipid-rich or peptide-rich regions and fitting to the reference spectra by means of least-squares refinement (Wang et al. 2009).

Results and discussion

Single amino acid replacement changes membrane activity of latarcin 2a

In a membrane-mimicking environment ltc2a adopts a helix–hinge–helix structure, with the first (residues 3–9) and the second (residues 13–21) helical regions connected by a poorly ordered fragment containing a helix-disrupting amino acid, glycine (Dubovskii et al. 2006). The two helices of the peptide differ in their hydrophobic organization. The N-terminal helix is strongly amphiphilic. The side-chains of hydrophobic (Phe3, Leu6, and Ile7) and hydrophilic (Lys5, Lys8, and Lys9) amino acids are divided and on opposite sides (Fig. 1, Dubovskii et al. 2006). The C-terminal helix is less amphiphilic, with a narrow hydrophobic segment composed of Ile15, Val19, and Ala22 (Fig. 1). It is of interest to investigate how modifications in the hinge affect the activity of latarcin 2a. Replacement of Gly11 with leucine was shown to significantly alter the hydrophobic properties of the peptide, leading to an increase of overall peptide toxicity (Polyansky et al. 2009). Replacement of glycine with alanine at position 11 only slightly increases the peptide's overall hydrophobicity, since the hydrophobicity indexes for the two amino acids are close (Eisenberg et al. 1982). At the same time, it is possible that the mutation affects the peptide's conformation, since alanine has much higher propensity to form a helix in membrane environments than glycine (Li and Deber 1994) and most definitely decreases the peptide's overall flexibility due to a much more restricted set of allowed dihedral (ϕ, ψ) angles for alanine. It is therefore expected that, in membrane-mimicking environments, the derivative ltc2aG11A will adopt a more rigid structure with a single hydrophobic segment extending from Phe3 to Ala22 (Fig. 1).

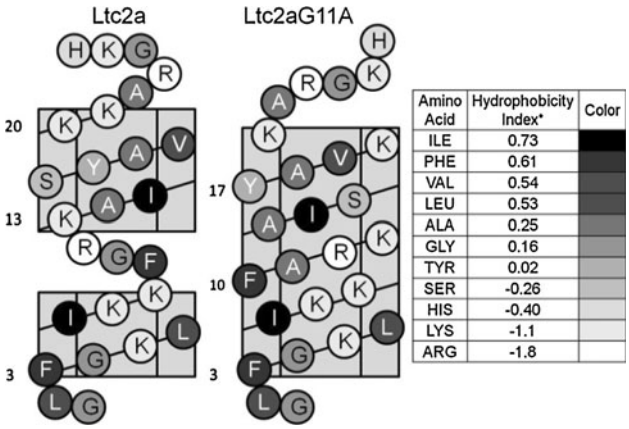

Fig. 1 Helical net diagrams for ltc2a and ltc2aG11A. Eisenberg consensus hydrophobicity scale was used (Eisenberg et al. 1982)

When a monolayer of phospholipid is deposited at the interface prior to peptide injection, the peptide's affinity to a cell membrane can be studied (Maget-Dana 1999; Brockman 1999). After injection into the subphase, a portion of the peptide's molecules will bind to and insert into the lipid, thus affecting the lipid film surface pressure. The degree of the pressure change depends on the initial pressure, the type of lipid used, the surface activity, and the concentration of the peptide. Figure 2 shows the result of this experiment where the surface pressure increase, $\Delta\pi$, after peptide addition (at the critical micellar concentration, determined in a separate experiment) is measured as a function of the initial lipid film pressure, π. The peptide concentrations were chosen. Two lipid systems were used: zwitterionic DPPC and anionic DPPG (Fig. 2). The dependencies, $\Delta\pi(\pi)$, were found to be slightly different for the two peptides. The critical pressures of insertion were determined by extrapolating the initial pressure, π, for surface pressure increase, $\Delta\pi$, equal to zero. In the case of zwitterionic DPPC, the critical pressures of insertion were found to be 35 ± 2 mN/m for ltc2aG11A and 28 ± 2 mN/m for ltc2a. The higher CPI value found for ltc2aG11A is likely due to its structure and, as a result, amphiphilic differences between ltc2a and ltc2aG11A. The natural cell membrane is believed to have a surface pressure in the 25–35 mN/m range (Ambroggio et al. 2004), suggesting

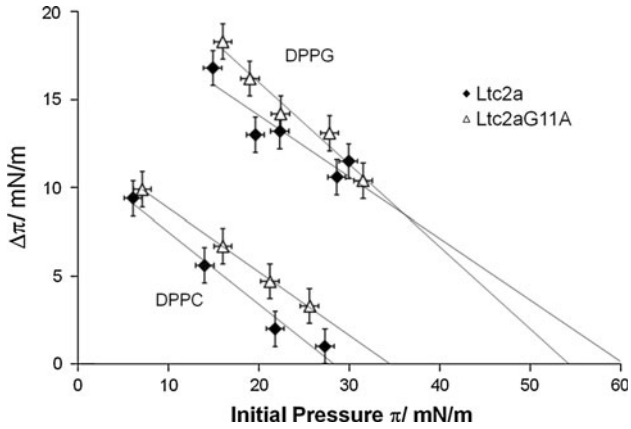

Fig. 2 Insertion of ltc2a (*filled diamonds*) and ltc2aG11A (*triangles*) into DPPC and DPPG monolayers. The surface pressure increase of the lipid monolayer ($\Delta\pi$) is presented as a function of the initial pressure (π). Extrapolation to zero $\Delta\pi$ gives the critical pressure of insertion (CPI). Peptide concentrations were 1.9 μg/ml (ltc2a) and 1.7 μg/ml (ltc2aG11A). Pressure measurements error is ±1 mN/m

that, of the two latarcin 2a derivatives, ltc2aG11A is more likely to spontaneously insert into zwitterionic cell membranes and is expected to be more toxic to mammalian cells. When considering the binding to anionic lipid DPPG, however, the critical pressures of insertion were found to be essentially the same for the two peptides (within experimental errors), since there is no difference in charge between the peptides: 55 ± 5 mN/m for ltc2aG11A and 60 ± 5 mN/m for ltc2a. These pressures are substantially greater than for DPPC, indicating the importance of electrostatic interactions in interactions of both latarcin derivatives with cell membrane.

Another interesting observation can be made from Fig. 3, which presents the time course of the surface pressure change, measured after peptide injection into the subphase under the phospholipid monolayers with surface pressure maintained constant between 20 and 30 mN/m. The graphs indicate that, after the initial, relatively fast association step that lasts 2–3 min and results in the surface pressure increase, a second, slower step can be detected, where the surface pressure for the lipid–peptide system decreases over an extended period of time. Since such behavior is only observed when a lipid monolayer is present, this second step can be attributed to slow lipid solubilization by the peptides, formation of micelles, and loss of lipid into the subphase. Such a trend is more pronounced for ltc2aG11A and with DPPG as lipid monolayer, likely due to higher concentration of adsorbed peptide at the anionic monolayer. This behavior is characteristic of the carpet mechanism of action for antimicrobial peptides (Gidalevitz et al. 2003), is consistent with the previously proposed model of action for ltc2a, and indicates the same mechanism for ltc2aG11A. Based on the results of the experiments described so far, the change associated with the replacement of Gly11 with Ala11 in ltc2a leads to a peptide ltc2aG11A that is capable of interacting and disrupting lipid monolayers via a carpet mechanism and that is more active against zwitterionic monolayers than the wild-type peptide.

Single amino acid replacement changes molecular surface area and lipid–peptide monolayer morphology

The pressure–area isotherms for monolayers of ltc2a, ltc2aG11A, DPPG, and DPPC in pure forms and in 50/50 lipid/peptide molar ratio mixtures are presented in Fig. 4. The lipid isotherms are shown as solid dark lines, the peptide isotherms are shown as grey dotted lines, and the mixture isotherms are presented as dashed lines. The isotherms of pure DPPC and DPPG, which have the same hydrophobic tail group but different hydrophilic head groups, are similar and show a transition from the liquid-expanded to the liquid-condensed phase at ~7 mN/m for DPPC (Ohe et al. 2004; Mansour et al. 2001; Kim et al. 2001) and at ~10 mN/m for DPPG (Ohe et al. 2004; Mansour et al. 2001; Vollhardt et al. 2000).

The compression isotherm for ltc2a shows two small but clearly distinguishable transition shoulders at ~7 mN/m and ~19 mN/m (Fig. 4, dotted lines, top). The mean area per molecule determined from the isotherm is ~180 Å^2. In the isotherm obtained for the modified latarcin, ltc2aG11A, one can also notice two small transition shoulders at ~12 and ~20 mN/m (Fig. 4, dotted lines, bottom), which are

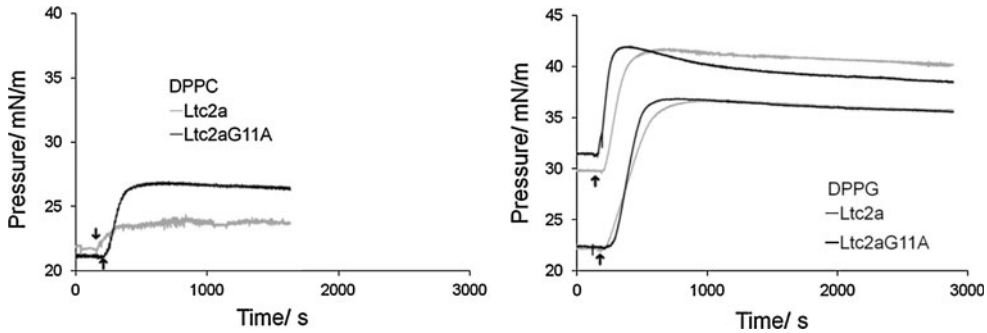

Fig. 3 Kinetics of ltc2a (*grey*) and ltc2aG11A (*black*) insertion into DPPC (*left*) and DPPG (*right*) monolayers. Peptide concentrations were 1.9 μg/ml (ltc2a) and 1.7 μg/ml (ltc2aG11A). *Arrows* indicate the moment of peptide injection

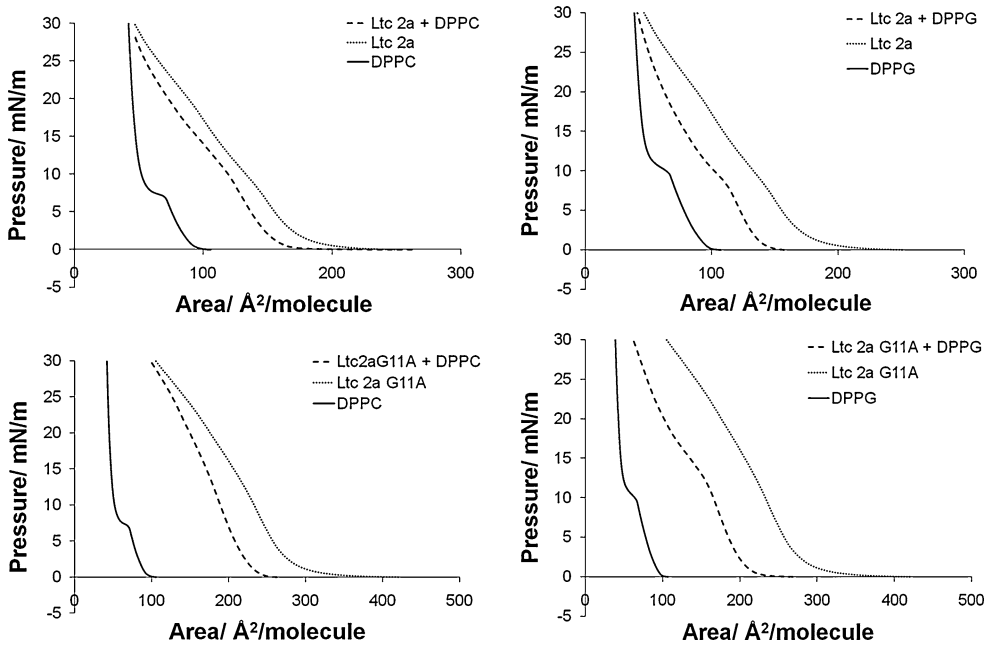

Fig. 4 *Top* compression isotherms for ltc2a, DPPC (*left*), DPPG (*right*), and 50:50% molar ratio mixtures of peptide and lipids. *Bottom* compression isotherms for ltc2aG11A, DPPC (*left*), DPPG (*right*), and 50:50% molar ratio mixtures of peptide and lipids

much less defined. The mean area occupied by a single ltc2aG11A molecule is found to be considerably larger at ~290 Å^2. The difference in the monolayer properties between the peptides is most likely related to the difference in the secondary structures of the peptides since, as discussed above, ltc2a forms a helix–hinge–helix conformation (Dubovskii et al. 2006) whereas ltc2aG11A likely forms a more rigid structure at the interface.

The length for a perfect α-helical conformation for a 26-amino-acid-residue peptide is estimated to be around 40.0 Å (1.5 Å of axial rise per residue) (Ambroggio et al. 2004). The length of the N-terminal helix of ltc2a is around 15.0 Å and that of the C-terminal helix is calculated to be 24.0 Å. If the estimated diameter of an average α-helix is 15 Å (5 Å for the helix core plus 5 Å for the side-chains surrounding the core, Ambroggio et al. 2004), the area occupied by a single ltc2aG11A molecule in a single-helix conformation with orientation parallel to the surface should be around 600 Å^2. If the molecule is perpendicular to the surface, the area is ~180 Å^2 (Ambroggio et al. 2004). Based on these calculations and the measured area per molecule of ltc2aG11A we can propose a model where the ltc2aG11A axis is either oriented at a ~60° angle relative to the interface, with the C-terminus inserted into the aqueous phase due to greater hydrophilicity, or does not form a single-helix conformation.

Areas occupied by the two helices in ltc2a are estimated to be ~290 Å^2 for the C-terminal helix and around 190.0 Å^2 for the N-terminal helix. This second value is close to the measured area per single ltc2a molecule in a monolayer, thus suggesting that during the compression the peptide rearranges itself so that the N-terminal helix is parallel to the surface and the C-terminal is pointing upwards. Such geometry, however, contradicts the proposed orientation of ltc2a in the membrane, where the C-terminal helix is found to be parallel to the interface (Dubovskii et al. 2006). Therefore, a suggested model of ltc2a arrangement in a monolayer is with the N-terminal helix perpendicular to the surface and the C-terminal helix tilted slightly to account for the smaller area. This model is supported by the hydrophobicity gradient present in the C-terminal helix that should promote the tilt of the helix. AFM topography imaging of monolayers containing peptide only and transferred onto mica at 7 and 30 mN/m surface pressure showed that, in monolayers, ltc2a and ltc2aG11A do not form aggregates (data not shown), thus validating the single-molecule calculations and data interpretation presented above.

Langmuir monolayer isotherms for the 50/50 peptide/lipid molar ratio mixtures show noticeable shoulders, suggesting either partial immiscibility or reorientation of the peptides during compression (Fig. 4, dashed lines; Oishi et al. 1997). The area per molecule obtained for the mixtures is found to be in between the areas of the pure peptide and the lipid, with area per molecule in monolayers containing DPPG being smaller than in DPPC, suggesting preferential interactions of both peptides with DPPG.

Detailed investigations of the peptide–lipid interactions are usually supported by calculations of the free energy of interactions (Maget-Dana 1999). In the case of latarcins, however, upon consecutive compression–expansion cycles, hysteresis between the compression and expansion isotherm is observed together with decrease of the area/molecule for all monolayers containing the peptides, making

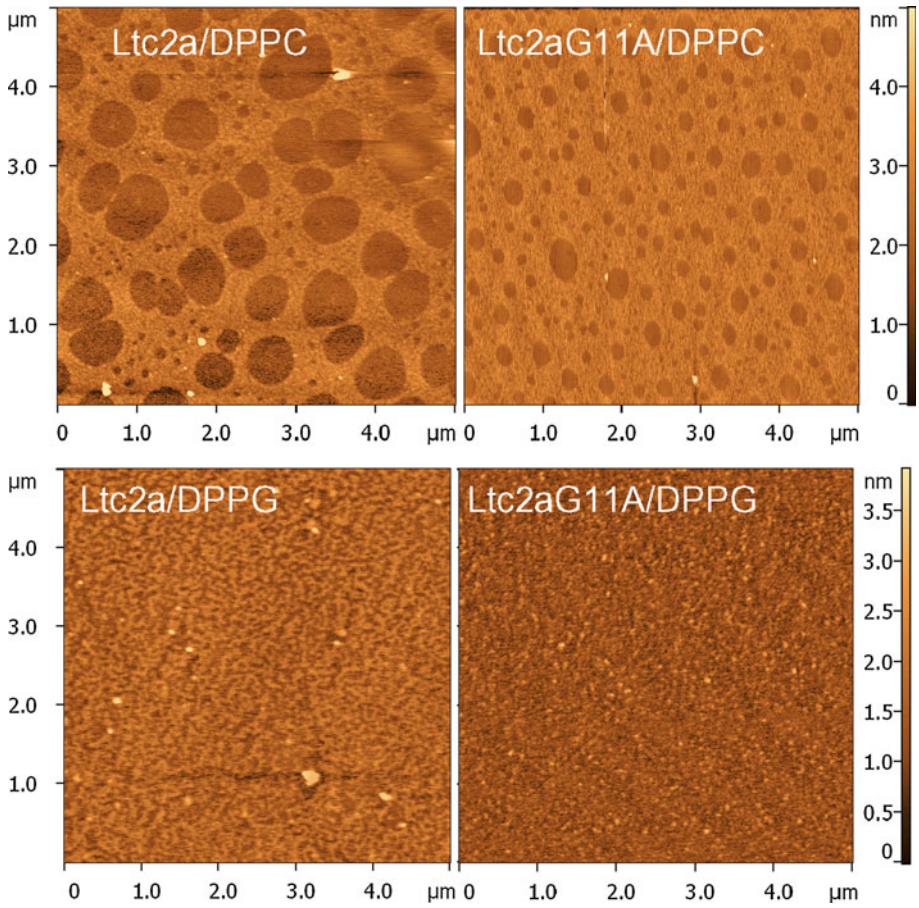

Fig. 5 Atomic force microscopy (AFM) images (5×5 µm^2) of ltc2a/DPPC, ltc2aG11A/DPPC, ltc2a/DPPG, and ltc2aG11A/DPPG mixture monolayers deposited at 30 mN/m. Lipid-to-peptide ratios are 1/1

calculation of the free energy of interactions rather challenging. We found that the hysteresis only appears when the monolayer is compressed above a pressure around 20 mN/m. Stable monolayers composed of amphiphilic molecules exhibit little hysteresis, indicating similarity of organization and disorganization of molecules during different compression and decompression cycles (Nakorn et al. 2007; Nakahara et al. 2006; Constantino et al. 1999) as is the case for pure DPPC and DPPG. It appears that monolayers containing the peptides are not stable above pressures of ~20 mN/m.

Upon compression above a certain pressure we observe not only hysteresis but also disappearance of certain features in the isotherms; for example, shoulders observed in the first compression no longer appear in the second compression (data not shown). Existence of large hysteresis can sometimes be related to molecular reorganization, but more often signals loss of peptide molecules from the air–water interface (Constantino et al. 1999; Pascholati et al. 2009). Comparison of the first expansion with the first compression reveals that some of the peptide molecules were forced into the subphase during the compression of the monolayer (Majerowicz et al. 2007; Minones et al. 2003). During the expansion, the peptide can be reincorporated into the monolayer. This reincorporation is not complete, which leads to a lower area per molecule on the second compression (Majerowicz et al. 2007; Minones et al. 2003).

To probe the lateral organization of the two peptides in lipid monolayers, the monolayers were transferred onto mica and AFM topography images were obtained (Fig. 5). There is a clear difference between the monolayers containing DPPC (Fig. 5, top) and DPPG (Fig. 5, bottom). In the case of zwitterionic DPPC, we observe circular domains between 100 nm and 500 nm in diameter and 1.3 nm lower than in the rest of the sample. These domains are considerably smaller with ltc2aG11A as compared with ltc2a. In contrast, no clear circular domains can be detected in monolayers with DPPG (Fig. 5, bottom). The monolayers are more homogeneous, although there are some small clusters observed. With DPPG, there is no considerable difference between ltc2a and ltc2aG11A. Thus, AFM data indicate that the peptides mix better and prefer to interact with anionic DPPG than with zwitterionic DPPC, which is expected for antimicrobial peptides.

To determine the nature of the circular domains we applied X-ray photoemission electron microscopy

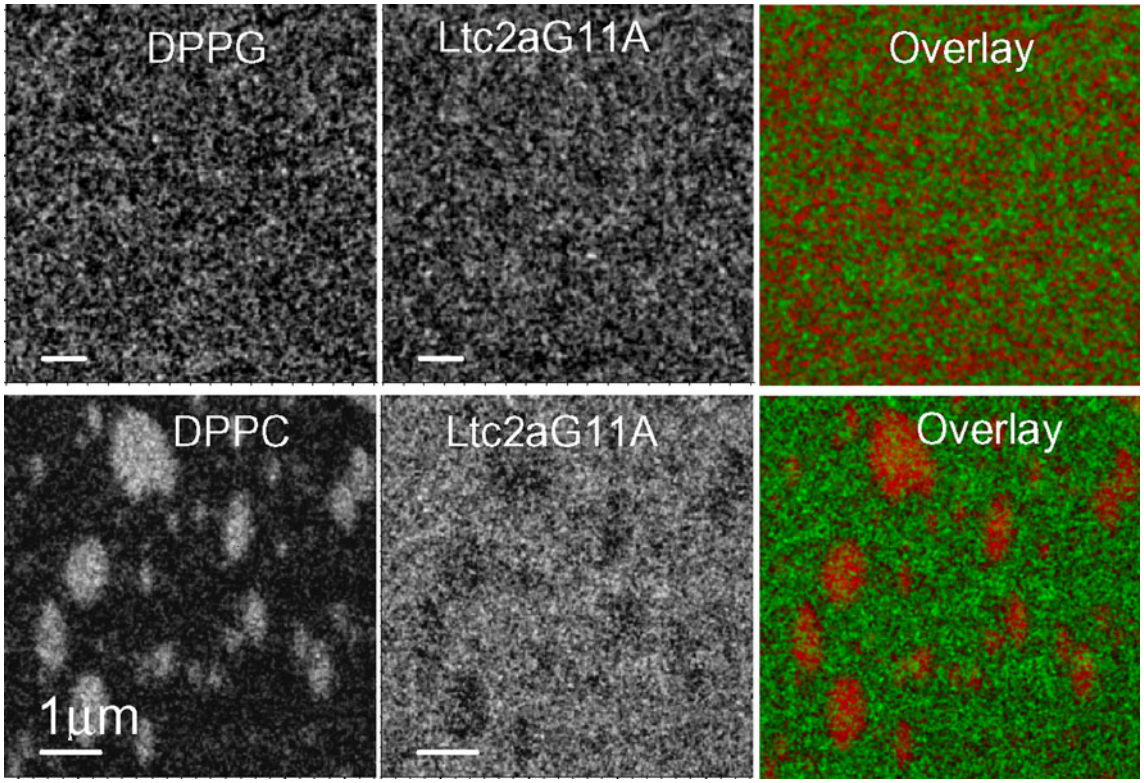

Fig. 6 X-ray photoemission electron microscopy (X-PEEM) images of DPPG, DPPC, ltc2aG11A, and overlays between the lipid and peptide signals. Lipid (DPPG or DPPC) is color-coded in *red*, and ltc2aG11A is color-coded in *green*. Lipid-to-peptide ratios are 1/1. *Scale bars* 1 µm

(X-PEEM), measuring C 1s image sequences. Component maps and color-coded composites (Fig. 6) show that in the DPPG/ltc2aG11A monolayer the peptide and the lipid are distributed homogeneously, indicating that the peptide mixes more readily with the DPPG lipid. At the same time, we detect clear separation between the peptide and the lipid components in the DPPC/ltc2aG11A monolayer. The circular domains that we observed in the AFM images appear to be mainly composed of the lipid, whereas the surrounding area is mainly peptide. The difference in the size of the circular domains for the two peptides can be explained by a slightly higher affinity of peptide ltc2aG11A to the zwitterionic monolayer, promoting hydrophobic interactions with DPPC.

The quantitative results from the NEXAFS least-squares refinement reveal that the composition of DPPG/ltc2G11A monolayer is $\sim 50 \pm 5{:}50 \pm 5\%$ DPPG:ltc2G11A, which may possibly indicate either homogeneous mixing of lipid and peptide or a mechanism where the peptide is positioned above the lipid. In contrast, for DPPC/ltc2G11A, the lipid-rich domains are composed almost entirely of lipid ($94 \pm 5{:}6 \pm 5\%$ DPPC:ltc2G11A) while the matrix is composed of $44 \pm 5{:}56 \pm 5\%$ DPPC:ltc2G11A. The presence of DPPC-rich domains reveals that the peptide mixes less readily with DPPC compared with DPPG, supporting the results obtained by AFM.

The length difference between a single DPPC lipid molecule (2.5 nm) and a single peptide molecule (4.0 nm) corresponds well to the measured height difference between the lipid and the peptide domains (1.3 nm, Fig. 5 top), supporting the above-proposed model of peptide insertion into DPPC monolayer with the N-terminal helix perpendicular to the surface and the C-terminal helix slightly tilted.

Modified latarcin creates more defects in phase-separated supported phospholipid bilayer models of mammalian cell membrane

Since modified latarcin ltc2aG11A was found to have a slightly higher affinity to zwitterionic monolayer as compared with the wild-type peptide, it was of interest to investigate the interaction of both latarcin derivatives with supported phospholipid bilayers that are often used to model cell membranes. One particular model of mammalian cell membrane that has been extensively used in the past 10 years is the so-called raft mixture, composed of DOPC, sphingomyelin, and cholesterol (Shaw et al. 2006, 2008; Ira and Johnston 2008). Supported bilayers prepared from DOPC/SPM/Chol mixture show phase separation, with SPM/Chol forming a higher gel phase and DOPC a lower fluid phase. AFM topography images obtained for

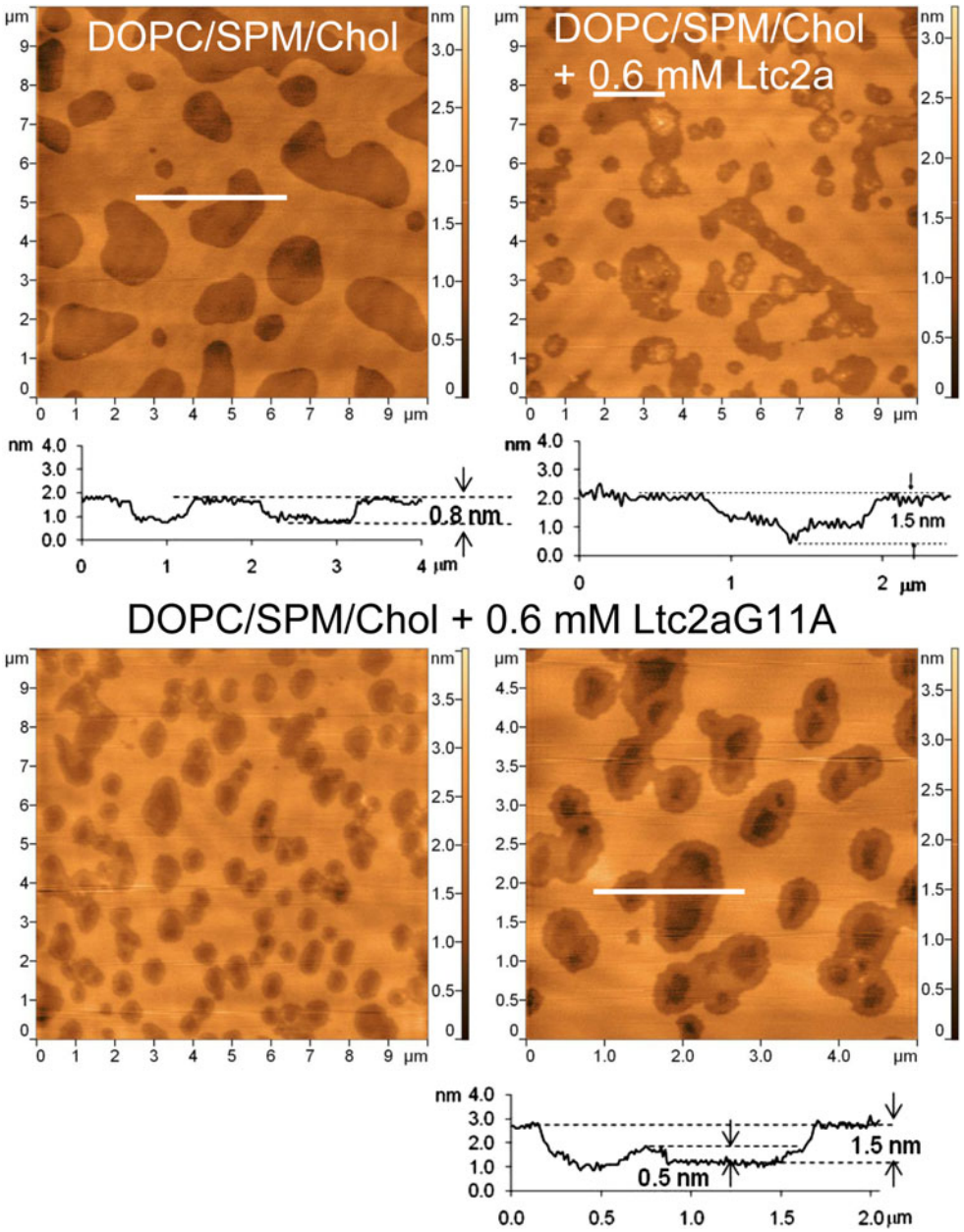

Fig. 7 Atomic force microscopy images of the DOPC/SPM/Chol 1/1/1 bilayer (*top left*), DOPC/SPM/Chol 1/1/1 bilayer after 30 min incubation with ltc2a [1.9 μg/ml (~0.6 μM), *top right*], and DOPC/SPM/Chol 1/1/1 bilayer after 30 min incubation with ltc2aG11A [1.9 μg/ml (~0.6 μM), *bottom*]

such bilayers (Fig. 7) show the phase separation, with height difference between the two phases of around 1 nm.

After incubating the bilayer with the peptides for 30 min, we observe considerable changes in the bilayer topography. First of all, there is spatial reorganization of the fluid phase domains for both peptides (Fig. 7). The lower fluid phase domains become considerably smaller. Secondly, the wild-type peptide induces formation of some small defects in the bilayer fluid phase (Fig. 7), which are 1.5 nm deeper than the gel phase. On the other hand, for ltc2aG11A these defects are considerably larger, and essentially occupy the entire fluid phase in the bilayer, with the exception of a narrow area near the domain edges (Fig. 7). Since the bilayer thickness is on the order of 5 nm and no defects of 5 nm depth are found, we can conclude that 1.9 μg/ml (~0.6 μM) concentration is insufficient to induce bilayer disruption. On the other hand, this peptide concentration is sufficient to induce membrane thinning. Such behavior was observed for other antimicrobial peptides and was explained by either interdigitation of bilayer, formation of single leaflet–peptide complex, or formation of asymmetric gel–fluid bilayer by lipid flip-flop (Shaw et al. 2006). At the moment we are unable to propose the exact mechanism by which latarcin 2a and its derivative induce membrane thinning. However, it is clear that the modified peptide ltc2aG11A has more disrupting effect on

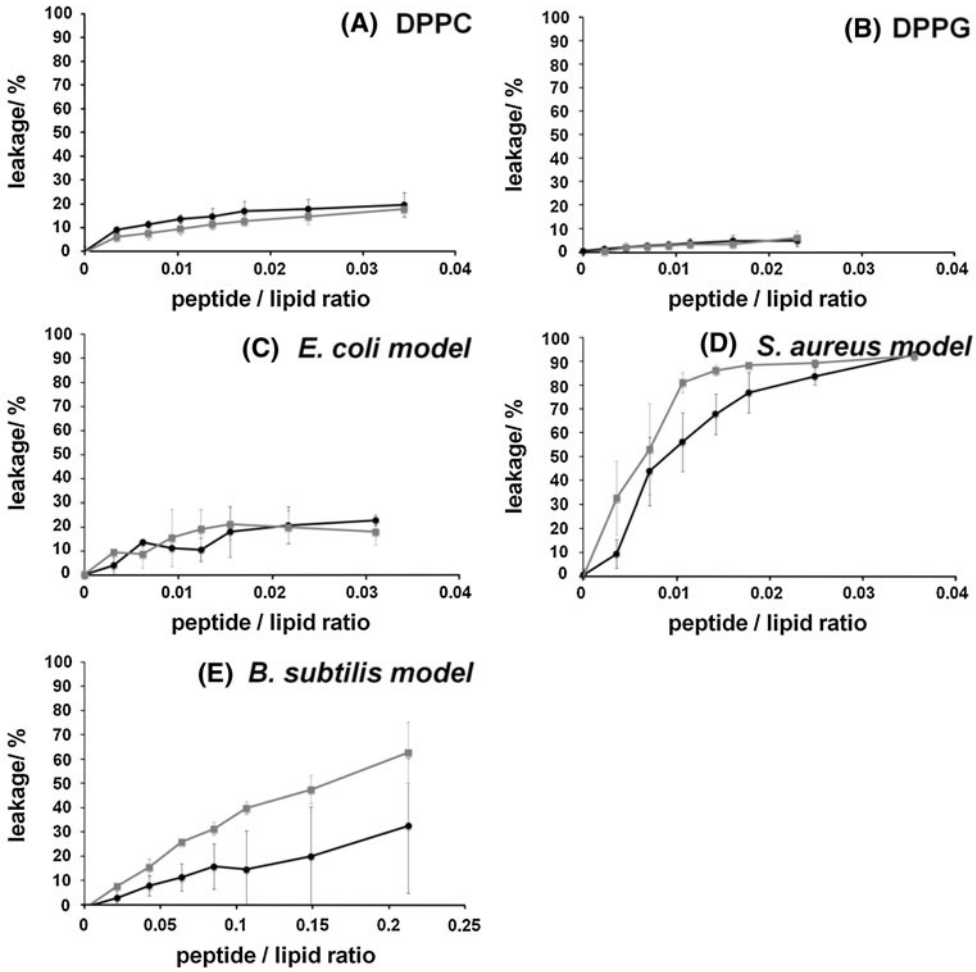

Fig. 8 Carboxyfluorescein fluorescence signal increase after addition of ltc2a (*black circles*) and ltc2aG11A (*grey squares*) into DPPC (**a**), DPPG (**b**), *E. coli* model (**c**, DOPE/DOPG 80/20 mol%), *S. aureus* model (**d**, DOPG/CL 55/45 mol%), and *B. subtilis* model (**e**, DOPE/DOPG/CL 12/84/4 mol%)

the mammalian model cell membrane than the wild-type latarcin, likely due to the difference in the structure.

Modification in the hinge region does not affect bacterial membrane rupturing activity

Finally, membrane rupturing activity of the peptides was studied using the carboxyfluorescein leakage assay (Fig. 8). Both peptides were found to induce leakage at low peptide/lipid ratios from all five model cell membranes used. Moderate lytic activity to zwitterionic vesicles (DPPC) was observed for both peptides. This information is consistent with the relatively high hydrophobicity of the peptides and high hemolytic activity (Dubovskii et al. 2006, 2008; Polyansky et al. 2009). Surprisingly, both peptides were found to be less lytic to DPPG than DPPC as well as other types of vesicles studied, suggesting non-additivity of electrostatic and hydrophobic interactions. This indicates that, although electrostatic interactions are important for initial recognition and binding of latarcins to the cell membrane, hydrophobic interactions play a crucial role in the peptides' lytic activity. The modified latarcin ltc2aG11A was found to be slightly more lytic to vesicles modeling Gram-positive bacteria *S. aureus* (55% DOPG/45% CL) and *B. subtilis* (12% DOPE/84% DOPG/4% CL) membranes, whereas no difference in activity between the peptides was found against Gram-negative bacteria *E. coli* (80% DOPE/20% DOPG) model membrane. The peptide activity was also found to correlate with the content of CL, thus suggesting that, in addition to simple electrostatic interactions, local membrane curvature, fluidity, and ability to form hydrogen bonds may play a considerable role in the activity of latarcin 2a (Domenech et al. 2009).

The data presented in this work correlate with previous studies, proposing a carpet mode of action for both ltc2a (Dubovskii et al. 2006) and ltc2aG11A. In this respect, it is interesting to note that, even though the modified ltc2aG11A is likely more rigid and could probably adopt a single-helix conformation in membrane-mimicking environments, which would be structurally similar to a different member of the latarcin family ltc1, the mechanism of action remains the same as for the helix–hinge–helix

peptide. Acting by the same mechanism suggests that, for latarcins, overall hydrophobicity and the pattern of hydrophobic residue distribution within the peptide α-helix are determining factors for the mechanism of action. Several analogs with point mutations in latarcin 2a were proposed to change the hydrophobic properties of the N-terminal helix (Polyansky et al. 2009). For several derivatives the selective toxicity towards bacterial cells was improved. One derivative with replacement of leucine with glycine at position 11 (ltc2aG11L) appeared to possess similar antibacterial properties to the wild-type ltc2a. At the same time it was shown to be considerably more toxic to mammalian cells. In membrane-mimicking environments both leucine and alanine are known to be helix-forming amino acids (Li and Deber 1994). Therefore, the overall physicochemical properties of ltc2aG11L and ltc2aG11A are very similar in terms of predicted secondary structure and hydrophobic residue distribution. It is reasonable to assume that ltc2aG11A is also characterized by an increased hemolytic activity which correlates with the stronger interactions of the peptide with zwitterionic model cell membranes as shown in the present work.

Deletion of the hinge region in helix–hinge–helix peptides has been shown to affect peptides' antimicrobial and cytotoxic properties (Polyansky et al. 2009; Oh et al. 2000; Pukala et al. 2004; Lee et al. 2007); for example, the antibiotic activity of caerin 1.1, a peptide that adopts a helix–hinge–helix conformation and acts through a carpet-like mechanism, decreased dramatically when two hinge-forming proline residues were replaced with alanines (Pukala et al. 2004). As a result, the peptide was shown to adopt a single rigid helix without a clear hydrophobic face, thus making the derivative less amphipathic and therefore less active. Replacement of two glycine amino acids with alanines in the single-helix antimicrobial peptide piscidin 1 increases the hydrophobic moment of the peptide and as a result was shown to increase both the antibacterial and hemolytic activity of the peptide (Lee et al. 2007). However, when one of the glycines was replaced with proline, thus breaking the helix to form a helix–hinge–helix structure, the peptide showed considerably higher selectivity towards bacterial cells than the original piscidin. This increase in selectivity was explained by the increased flexibility of the peptide. Removal of the hinge sequence in a hybrid peptide incorporating cecropin and magainin 2 resulted in a single α-helical structure without amphiphilicity (Oh et al. 2000). The obtained derivative was found to possess significantly decreased bactericidal and tumoricidal activities. Replacement of Gly11 in ltc2a with alanine or leucine does not lead to loss of amphipathicity but does result in a much more rigid structure that interacts with zwitterionic model cell membranes more efficiently, thereby explaining its higher hemolytic activity.

Conclusions

In this work, we examined the role of the hinge in the ltc2a peptide in the membrane binding and lytic activity of the peptide. Collectively, the findings suggest that the strength and selectivity of the antimicrobial activity of ltc2a are principally dependent on the hinge found at the center of the peptide. It has been shown that nonspecific binding of antimicrobial peptides to the negatively charged DPPG monolayer is dependent on both hydrophobic and electrostatic interactions. These interactions provide selectivity and affinity to allow peptide accumulation on the bacterial membrane to induce disruption, resulting in wide-spectrum antimicrobial activity. This work has demonstrated that the linear derivative ltc2aG11A does exhibit different antibacterial properties compared with the helix–hinge–helix conformation of ltc2a and has suggested that ltc2aG11A should exhibit higher hemolytic and cytotoxic activities, while its antimicrobial properties remain similar to those of ltc2a.

Acknowledgments Financial support was provided by ERA, NSERC, and CFI. X-ray microscopy was carried out using the polymer STXM on beamline 5.3.2 and the magnetic X-PEEM on beamline 7.3.1 at the ALS, which is supported by the US DoE under contract DE-AC03-76SF00098. We thank David Kilcoyne and Tolek Tyliszczak (STXM532) as well as Andreas Scholl and Andrew Doran (PEEM2) for their diligence and expertise in keeping the beamlines in top condition.

References

Ambroggio EE, Separovic F, Bowie J, Fidelio GD (2004) Structure behaviour and peptide-lipid interactions of the antibiotic peptides, maculatin and citropin. Biochim Biophy Acta 1664:31–37

Brockman H (1999) Lipid monolayer: why use half a membrane to characterize protein-membrane interactions? Curr Opin Struct Biol 9:438–443

Brogden KA (2005) Antimicrobial peptides: pore formers or metabolic inhibitors in bacteria? Nature Rev Microbiology 3:238–250

Chakrabartty A, Baldwin JA, Baldwin RL (1991) Large differences in the helix propensities of alanine and glycine. Nature 351:586–588

Constantino CJL, Dhanabalan A, Oliveira ON (1999) Experimental artifacts in the surface pressure measurement for lignin monolayers in langmuir troughs. Rev Sci Instrum 70:3674–3680

Domenech O, Francius G, Tulkens PM, Van Bambeke F, Dufrene Y, Mingeot-Leclercq MP (2009) Interactions of oritavancin, a new lipoglycopeptide derived from vancomycin, with phospholipid bilayers: effect on membrane permeability and nanoscale lipid membrane organization. Biochim Biophys Acta Biomembr 1788:1832–1840

Dubovskii PV, Volynsky PE, Polyansky AA, Chupin VV, Efremov RG, Arseniev AS (2006) Spatial structure and activity mechanism of a novel spider antimicrobial peptide. Biochemistry 45:10759–10767

Dubovskii PV, Volynsky PE, Polyansky AA, Karpunin DV, Chupin VV, Efremov RG, Arseniev AS (2008) Three-dimensional structure/hydrophobicity of latarcins specifies their mode of membrane activity. Biochemistry 47:3525–3533

Eisenberg D, Weiss RM, Terwilliger TC, Wilcox W (1982) Hydrophobic moments and protein structure. Faraday Symp Chem Soc 17:109–120

Epand RF, Savage PB, Epand RM (2007) Bacterial lipid composition and the antimicrobial efficacy of cationic steroid compounds (Ceragenins). Biochim Biophys Acta 1768:2500–2509

Gidalevitz D, Ishitsuka Y, Muresanv AS, Konovalov O, Waring AJ, Lehrer RI, Lee KYC (2003) Interaction of antimicrobial peptide protegrin with biomembranes. Proc Natl Acad Sci 100:6302–6307

Guani-Guerra E, Santos-Mendoza T, Lugo-Reyes SO, Teran LM (2010) Antimicrobial peptides: general overview and clinical implications in human health and disease. Clin Immunol 135:1–11

Hancock REW, Sahl H-G (2006) Antimicrobial and host-defense peptides as new anti-infective therapeutic strategies. Nature Biotech 24:1551–1557

Ibrahim HR, Thomas U, Pellegrini A (2001) A helix-loop-helix peptide at the upper lip of the active site cleft of lysozyme confers potent antimicrobial activity with membrane permeabilization action. J Biol Chem 276:43767–43774

Ira P, Johnston LJ (2008) Spingomyelinase generation of ceramide promotes clustering of nanoscale domains in supported bilayer membranes. Biochim Biophys Acta 1778:185–197

Javadpour MM, Eilers M, Groesbeek M, Smith SO (1999) Helix packing in polytopic membrane proteins: role of glycine in transmembrane helix association. Biophys J 77:1609–1618

Kim K, Kim C, Byun Y (2001) Preparation of a dipalmitoylphosphatidylcholine/cholestrol langmuir-blodgett monolayer that suppresses protein adsorption. Langmuir 17:5066–5070

Koprinarov IN, Hitchcock AP, McCrory CT, Childs RF (2002) Quantitative mapping of structured polymeric systems using singular value decomposition analysis of soft X-ray images. J Phys Chem B 106:5358–5364

Kozlov SA, Vassilevski AA, Feofanov AV, Surovoy AY, Karpunin DV, Grishin EV (2006) Latarcins, antimicrobial and cytolytic peptides from the venom of the spider *Lachesana tarabaevi* (Zodariidae) that exemplify biomolecular diversity. J Biol Chem 281:20983–20992

Lee S-A, Kim YK, Lim SS, Zhu WL, Ko W, Shin SY, Hahm K-S, Kim Y (2007) Solution structure and cell selectivity of piscidin 1 and its analogues. Biochemistry 46:3653–3663

Leung BO, Hitchcock AP, Cornelius R, Brash JL, Scholl A, Doran A (2009) An X-ray spectromicroscopy study of protein adsorption to a polystyrene-polylactide blend. Biomacromolecules 10:1838–1845

Li S-C, Deber CM (1994) A measure of helical propensity for amino acids in membrane environments. Nat Struct Mol Biol 1:368–373

Liu ZH, Qian W, Li J, Zhang Y, Liang S (2009) Biochemical and pharmacological study of venom of the wolf spider Lycosa singoriensis. J Venom Anim Toxins incl Trop Dis 15:79–92

Maget-Dana R (1999) The monolayer technique: a potent tool for studying the interfacial properties of antimicrobial and membrane-lytic peptides and their interactions with lipid membrane. Biochim Biophys Acta 1462:109–140

Majerowicz M, Waring AJ, Wen S, Bringezu F (2007) Interaction of the antimicrobial peptide dicynthaurin with membrane phospholipids at the air-liquid interface. J Phys Chem B 111:3813–3821

Mansour H, Wang D, Chen C, Zografi G (2001) Comparison of bilayer and monolayer properties of phospholipid systems containing dipalmitoylphosphatidylglycerol and dipalmitoylphosphatidylinositol. Langmuir 17:6622–6632

Melo MN, Ferre R, Castanho M (2009) Antimicrobial peptides: linking partition, activity and high membrane-bound concentrations. Nat Rev Microbiol 7:245–250

Minones J Jr, Dynarowicz-Latka P, Minones J, Rodrigez Patino JM, Iribarnegaray EJ (2003) Orientational changes in dipalmitoyl phosphatidyl glycerol langmuir monolayers. J Colloid Interface Sci 265:380–385

Nakahara H, Lee S, Sugihara G, Shibata O (2006) Mode of interaction hydrophobic amphiphilic α-helical peptide/dipalmitoylphosphatidylcholine with phosphatidyglycerol or palmitic acid at the air-water interface. Langmuir 22:5792–5803

Nakorn PN, Meyer MC, Flach CR, Mendelson R, Galla H-J (2007) Surfactant protein C and lung function: new insights into the role of ·-helical length and palmitoylation. Eur Biophys J 36:477–489

Oh D, Shin SY, Lee S, Kang JH, Kim SD, Ryu PD, Hahm K, Kim Y (2000) Role of the hinge region and the tryptophan residue in the synthetic antimicrobial peptides, cecropin A(1-8)-magainin 2(1-12) and its analogues, on their antibiotic activities and structures. Biochemistry 39:11855–11864

Ohe C, Ida Y, Matsumoto S, Sasaki T, Goto Y, Noi M, Tsurumaru T, Itoh K (2004) Investigations of polymyxin B-phospholipid interactions by vibrational sum frequency generation spectroscopy. J Phys Chem B 108:18081–18087

Oishi Y, Takashima Y, Suehiro K, Kajiyama T (1997) Effect of ionic repulsion among hydrophilic groups on aggregation structure of fatty acid monolayer on the water surface. Langmuir 13:2527–2532

Okamoto Y, Hansmann UHE (1995) Thermodynamics of helix-coil transitions studied by multicanonical algorithms. J Phys Chem 99:11276–11287

Pascholati CP, Lopera EP, Pavinatto FJ, Caseli L, Nobre TM, Zaniquelli MED, Viitala T, D'Silva C, Oliveira ON Jr (2009) The interaction of an antiparasitic peptide active against African sleeping sickness with cell membrane. Colloids Surf B Biointerfaces 74:504–510

Polyansky AA, Vassilevski AA, Volynsky PE, Vorontsova OV, Samsonova OV, Egorova NS, Krylov NA, Feofanov AV, Arseniev AS, Grishin EV, Efremov RG (2009) N-terminal amphipathic helix as a trigger of hemolytic activity in antimicrobial peptides: a case study in Latarcins. FEBS Lett 583:2425–2428

Pukala TL, Brinkworth CS, Carver JA, Bowie JH (2004) Investigating the importance of the flexible hinge in caerin 1.1: solution structures and activity of two synthetically modified caerin peptides. Biochemistry 43:937–944

Pukala TL, Boland MP, Gehman JD, Kuhn-Nentwig L, Separovic F, Bowie JH (2007) Solution structure and interaction of cupiennin 1a, a spider venom peptide, with phospholipid bilayers. Biochemistry 46:3576–3585

Reddy KV, Yedery RD, Aranha C (2004) Antimicrobial peptides: premises and promises. Int J Antimicrob Agents 24:536–547

Rohl CA, Fiori W, Baldwin RL (1999) Alanine is helix-stabilizing in both template-nucleated and standard peptide helices. Proc Natl Acad Sci USA 96:3682–3687

Shaw JE, Alattia J-R, Verity JE, Prive GG, Yip CM (2006) Mechanisms of antimicrobial peptide action: studies of indolicidin assembly at model membrane interfaces by in situ atomic force microscopy. J Struct Biol 154:42–58

Shaw JE, Epand RF, Hsu JCY, Mo GCH, Epand RM, Yip CM (2008) Cationic peptide-induced remodeling of model membranes: direct visualization by in situ atomic force microscopy. J Struct Biol 162:121–138

Shlyapnikov YM, Andreev YA, Kozlov SA, Vassilevski AA, Grishin EB (2008) Bacterial production of latarcin 2a, a potent antimicrobial peptide from spider venom. Prot Exp Pur 60:89–95

Stewart-Ornstein J, Hitchcock AP, Hernàndez-Cruz D, Henklein P, Overhage J, Hilpert K, Hale J, Hancock REW (2007) Using intrinsic X-ray absorption spectral differences to identify and map peptides and proteins. J Phys Chem B 111:7691–7699

Van Khan EJM, van der Bent AR, Demel R, de Kruijff B (2001) Membrane activity of the peptide antibiotic clavanin and the importance of its glycine residues. Biochemistry 40:6398–6405

Vollhardt D, Fainerman VB, Siegel S (2000) Interfacial rate processes in adhesion and friction. J Phys Chem B 104:4115–4121

Wang J, Li L, Morin C, Hitchcock AP, Doran A, Scholl A (2009) Radiation damage in soft X-ray microscopy. J Electron Spectrosc Relat Phenom 170:25–36

Won A, Ianoul A (2009) Interactions of antimicrobial peptide from C-terminus of myotoxin II with phospholipid mono- and bilayers. Biochim Biophys Acta 1788:2277–2283

Yeaman MR, Yount NY (2003) Mechanisms of antimicrobial peptide action and resistance. Pharm Rev 5:27–55

Zasloff M (2002) Antimicrobial peptides of multicellular organisms. Nature 415:389–395

Zhang L, Falla TJ (2010) Potential therapeutic application of host defense peptides. Methods Mol Biol 618:303–327